Journal Pre-proof

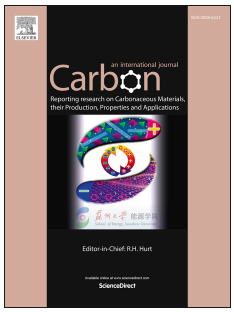

Enhanced Graphitization of CO_2-Derived Carbon Anodes via Joule Heating Reformation for High-Performance Lithium-Ion Batteries

Minghao Liu, Hao Shi, Lei Guo, Zhouyu Fang, Di Chen, Wenmiao Li, Bowen Deng, Wei Li, Kaifa Du, Huayi Yin, Dihua Wang

PII: S0008-6223(24)01000-5

DOI: https://doi.org/10.1016/j.carbon.2024.119781

Reference: CARBON 119781

To appear in: *Carbon*

Received Date: 5 August 2024

Revised Date: 16 October 2024

Accepted Date: 29 October 2024

Please cite this article as: M. Liu, H. Shi, L. Guo, Z. Fang, D. Chen, W. Li, B. Deng, W. Li, K. Du, H. Yin, D. Wang, Enhanced Graphitization of CO_2-Derived Carbon Anodes via Joule Heating Reformation for High-Performance Lithium-Ion Batteries, *Carbon*, https://doi.org/10.1016/j.carbon.2024.119781.

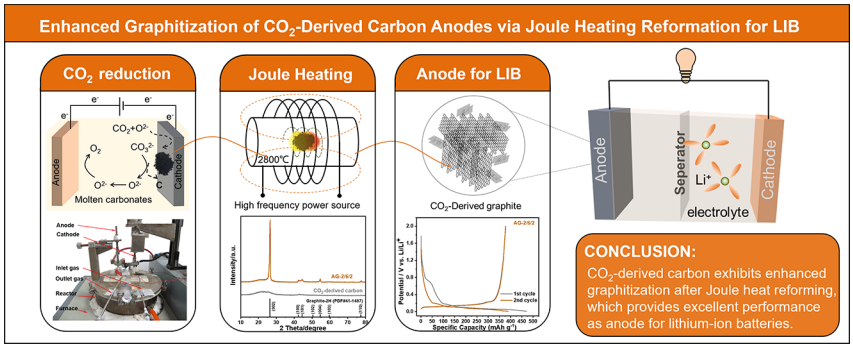

Enhanced Graphitization of CO_2-Derived Carbon Anodes via Joule Heating Reformation for High-Performance Lithium-Ion Batteries

Minghao Liu[a,b], Hao Shi[a,b], Lei Guo[a,b], Zhouyu Fang[a,b], Di Chen[a,b], Wenmiao Li[a,b*], Bowen Deng[a,b], Wei Li[a,b], Kaifa Du[a,b*], Huayi Yin[a,b], Dihua Wang[a,b*]

Affiliations:

[a] School of Resource and Environmental Sciences, Wuhan University, Wuhan 430072, China.

[b] Hubei International Scientific and Technological Cooperation Base of Sustainable Resources and Energy, Wuhan 430072, China.

[*]Corresponding author. E-mail: wangdh@whu.edu.cn (D.W.); dukf@whu.edu.cn (K.D.); liwenmiao@whu.edu.cn (W.L.).

Abstract:

Molten salt electrolysis of CO_2 represents a promising technology for highly efficient CO_2 capture and the production of economically valuable CO_2-derived carbon materials. In this study, we established a 100-ampere-scale molten salt CO_2 electrolysis cell to synthesize hundreds of grams of CO_2-derived carbon. Subsequent Joule heating at 2800 ^oC transformed these materials into high-quality graphite. Further composite modification with asphalt and petroleum coke effectively reduced surface area, resulting in high performance graphite for lithium-ion battery. The CO_2-derived graphite anodes demonstrated high reversible capacities ranging from 297.7 to 378.1 mAh g^{-1}, exhibiting outstanding rate capability and stability over 300 charge-discharge cycles at a current density of 1 A g^{-1}. Finally, we assembled a coin full-cell using AG-2/2/6 anode and LFP cathode, which demonstrated good cycling performance. XPS analysis revealed a significant reduction in oxygen content by the post-reformation, facilitating the formation of highly graphitized structures. This study not only pioneers the up-class synthesis of CO_2-derived carbon but also underscores its potential for sustainable energy applications, particularly in lithium-ion battery technology.

Keywords: CO_2-derived carbon, Joule heating reformation, Graphite anode, Lithium-ion battery, Molten salt electrolysis.

1. Introduction

The synthesis of carbon materials from CO_2 via molten salt electrolysis represents a transformative technology with significant promise for addressing environmental challenges and advancing sustainable energy solutions[1-3]. This method boasts several distinct advantages, including high CO_2 capture efficiency, superior selectivity of cathodic products, and high current density[4-7], positioning it as a viable candidate for large-scale applications in the high-value utilization of CO_2. Unlike traditional aqueous electrolysis methods, molten salt electrolysis excels in producing economically valuable CO_2-derived carbon directly at the cathode[8,9]. Extensive research efforts over the years have demonstrated the versatility of this technology in synthesizing a wide range of CO_2-derived carbon. These include carbon nanotubes[10,11], carbon nanofibers, carbon spheres, nanoparticles[12], porous carbons[13], graphene[14,15], and graphite flakes[16,17]. Each of these materials holds significant economic value, which is crucial for the widespread commercialization of this technology. Therefore, identifying optimal applications for these CO_2-derived carbons is paramount.

Recently, technologies related to lithium-ion batteries have been rapidly advancing[18,19].Carbon-based materials play a pivotal role as anode materials in lithium-ion batteries due to their high market value and substantial growth potential[20-22]. Currently, the primary sources of carbon-based anodes—petroleum coke[23,24], pitch[25], and natural graphite[26,27]—are non-renewable resources facing sustainability challenges. Utilizing carbon materials synthesized through molten salt electrolysis of CO_2 as anode materials for lithium-ion batteries not only realizes the high-value utilization of CO_2 but also mitigates supply chain issues associated with conventional anode materials. The field has seen significant research progress. For

example, Groult et al.[28] achieved a specific capacity three times higher than theoretical graphite capacity using thermally treated CO_2-derived carbon as an anode material. Ge et al.[29] demonstrated a specific capacity of 215.5 mAh g^{-1} after 100 charge-discharge cycles with amorphous CO_2-derived carbon prepared in the LiCl–Li_2CO_3 system. Tang et al.[30] reported a specific capacity of 266 mAh g^{-1} at a current density of 500 mA g^{-1} using CO_2-derived carbon derived from a Li-Na-K_2CO_3 molten salt system at 450 °C.

Despite these advancements, integrating CO_2-derived carbon into lithium-ion batteries faces several challenges. These include the lack of a distinct voltage plateau for lithium storage and low initial Coulombic efficiency. The insufficient graphitization degree of carbon materials hinders effective Li^+ intercalation[31], while their high specific surface area leads to excessive Li^+ consumption during the formation of the solid electrolyte interface (SEI) film, thereby reducing initial Coulombic efficiency[32].

To address these challenges, this study focuses on enhancing the graphitization degree of CO_2-derived carbon through Joule heating reformation. The common method for increasing the graphitization degree of carbon materials is high-temperature thermal reformation. The Joule heating reforming method has advantages over traditional thermal reforming methods, including high energy conversion efficiency, rapid and uniform heating, and reduced oxidation[33,34]. Additionally, during the graphitization process of carbon materials, asphalt is typically added as a binder to reduce the specific surface area while enhancing the degree of graphitization[35]. petroleum coke is a common precursor for graphite anodes; however, needle coke with high crystallinity demonstrates high capacity but relatively poor rate performance. Therefore, we aimed to use asphalt as a "bridge" to combine the high-capacity characteristics of petroleum coke with the high electrical conductivity of CO_2-derived carbon, ultimately developing an anode material with both high capacity and high rate performance.

Based on the above, we first designed a 100-ampere-scale molten salt CO_2 electrolysis cell to efficiently produce hundreds of grams of CO_2-derived carbon.

Subsequently, the obtained amorphous CO_2-derived carbon was subjected to Joule heating at 2800 °C to transform it into graphite materials with high graphitization crystallinity. These materials were further prepared in composite form with asphalt and petroleum coke to create graphite anode materials for lithium-ion batteries with lower surface area. The prepared graphite anodes exhibited outstanding reversible capacity (297.7~378.1 mAh g^{-1}), initial Coulombic efficiencies (72.6%~80.5%), and rate capability. Moreover, it demonstrated excellent cycling stability, maintaining nearly undiminished capacity after 300 cycles at a current density of 1A g^{-1}. Finally, we assembled a coin full-cell using AG-2/2/6 anode and LFP cathode, which demonstrated good cycling performance. This research not only advances the fundamental understanding of carbon materials synthesized via molten salt electrolysis of CO_2 but also aims to overcome critical barriers to their practical application in high-performance lithium-ion batteries.

2. Materials and methods

2.1 Preparation of CO_2-derived carbon

30 kg of anhydrous Li_2CO_3-Na_2CO_2-K_2CO_3 eutectic salt (mixed in a molar ratio of 43.5:31.5:25.0) were placed in a titanium crucible (27 cm × 29.6 cm). The titanium crucible was then placed in a sealed stainless steel reactor, which was situated in a heating furnace. The molten salt mixture was dried at 300 °C for 12 h, followed by heating to 650 °C under an argon atmosphere until the salt was fully melted, and then held at this temperature. To assemble a 100-ampere-scale electrolysis cell, a pre-oxidized A3 steel plate (20 cm × 20 cm × 3 mm) was used as the oxygen evolution anode, a nickel plate (20 cm × 20 cm × 3 mm) served as the cathode, and a stainless steel powder sintered porous tube functioned as the CO_2 gas sparger. Electrolysis was conducted at a constant current of 100 A for 10 h using a computer-controlled DC power source (Shenzhen Neware Electronic Ltd., China), with the cell voltage

monitored throughout the process. The outlet gas was first passed through a condenser and then analyzed using a gas analyzer (AGA1000, Aut. EQ. Co. Ltd, China).

2.2 Preparation of CO_2-derived graphite

We weighed and mixed crushed asphalt with 100 g of kerosene, heating it to 150 °C until fully dissolved. Then, we sequentially added petroleum coke and CO_2-derived carbon, heating and stirring for 4 hours until the kerosene evaporated, forming a paste. The paste was placed in a crucible, heated at 2 °C min^{-1} to 500 °C in an argon atmosphere, and held for 6 hours to obtain the primary carbonization product. The primary carbonization product was then ground and treated at 2800 °C for 2 hours in an induction heating furnace, and cooled to obtain the sample. The product obtained by direct Joule heating reformation of CO_2-derived carbon was named EC-2800, and the product obtained by Joule heating reformation of a mixture of asphalt, petroleum coke, and CO_2-derived carbon in a 20:20:60 ratio was named AG-2/2/6. The AG sample refers to commercially purchased standard artificial graphite, which was used as a comparison.

2.3 Materials characterization

Phases of CO_2-derived carbon materials were identified by X-ray diffraction (XRD, Rigaku Mini Flex 600 with Cu Kα1radiationatλ =1.5405Å). Here, the Bragg's equation is introduced to calculate the interlayer spacing (d_{002}) of the obtained graphite materials from the position of the (002) peak in the XRD pattern.

$$d_{002} = \frac{\lambda}{2sin\theta} \quad (1)$$

$$g = \frac{0.3440 - d}{0.3440 - 0.3354} \times 100\% \quad (2)$$

where d_{002} denotes the interlayer spacing, λ is the wavelength of the X-ray, θ stands for the Bragg angle corresponding to the diffraction peak, g is the degree of graphitization of the graphite product, and 0.3354 and 0.3440 nm represent the interlayer distance of ideal single-crystal graphite and original carbonaceous materials, respectively.

Raman spectrometers were used to quantify the graphitization of carbon materials (Lab RAMHR Evolution) with a 532 nm wavelength. The oxygen and carbon contents of CO_2-derived carbon materials were determined using X-ray photoelectron spectroscopy (XPS, Thermo Scientific K-Alpha). The surface morphology of the CO_2-derived carbon materials was observed by scanning electron microscopy (SEM, TESCAN, Mira3 LMH) and Transmission Electron Microscope (TEM, FEI Tecnai G2 F20). Nitrogen adsorption and desorption isotherms were measured at -196 °C using a Micromeritics ASAP 2460 instrument. The specific surface area (SSA) of the sample was calculated using the BET (Brunauer-Emmett-Teller) method, and the pore size distribution was calculated using the Barret-Joymer-Hanlenda (BJH) method from the adsorption branches of the isotherms.

2.4 Electrochemical measurements

In half-cells, the experimental product was sealed into CR2032 coin cells with lithium foil as the negative electrode. The working electrode was prepared with the ratio 80:10:10 wt.% of active composite, polyvinylidene fluoride (PVDF) and conductive carbon black in N-methyl pyrrolidone (NMP) solvent. The active materials loading in the electrode is 1.2-1.5 mg cm^{-2}. In full-cells, We prepared the cathode LFP electrode with a composition of 92% active LFP material, 5% SP conductive agent, and 3% PVDF binder, maintaining a loading of approximately 2-3 mg cm^{-2}. The discs were 12 mm in diameter (same size as the anode), and the practical capacity of the LFP cathode was set at 160 mAh g^{-1} (at a current density of 0.1 C). The loading of the anode sheets ranged from 1.9 to 2.1 mg cm^{-2}. The designed N/P ratio was approximately 1.2 to 1.3. In a glovebox filled with argon, the cells were sealed with a celgard2400 membrane separator and 1.0 M lithium hexafluorophosphate ($LiPF_6$) in carbonate acetate (EC): diethyl carbonate (DEC) = 1:1 Vol% as electrolyte. A NEWARE Battery Test System (CT-4008TN, Shenzhen, China) is employed for calculating the galvanostatic charge/discharge tests at 25 °C. Cyclic voltammetry (CV) and electrochemical impedance spectra (EIS) were measured by the electrochemical workstation (Shanghai

Chenhua Instrument Co. Ltd., China) in the voltage window between 0.01 and 2.0 V and an alternating current amplitude of 5 mV in the frequency range of 100,000–0.01 Hz, respectively.

3. Results and discussions

3.1 Conversion of CO_2 to high-quality graphite via molten salt electrolysis and Joule heating reformation

Carbon dioxide (CO_2) is not only a major industrial waste gas contributing to severe environmental issues but also a valuable carbon resource[36]. In this study, CO_2 was converted into CO_2-derived carbon through a one-step molten salt capture and electrolysis process. This CO_2-derived carbon was then reformed into high-quality graphite material using high-frequency inductive Joule heating, achieving the conversion of CO_2 into high-quality graphite.

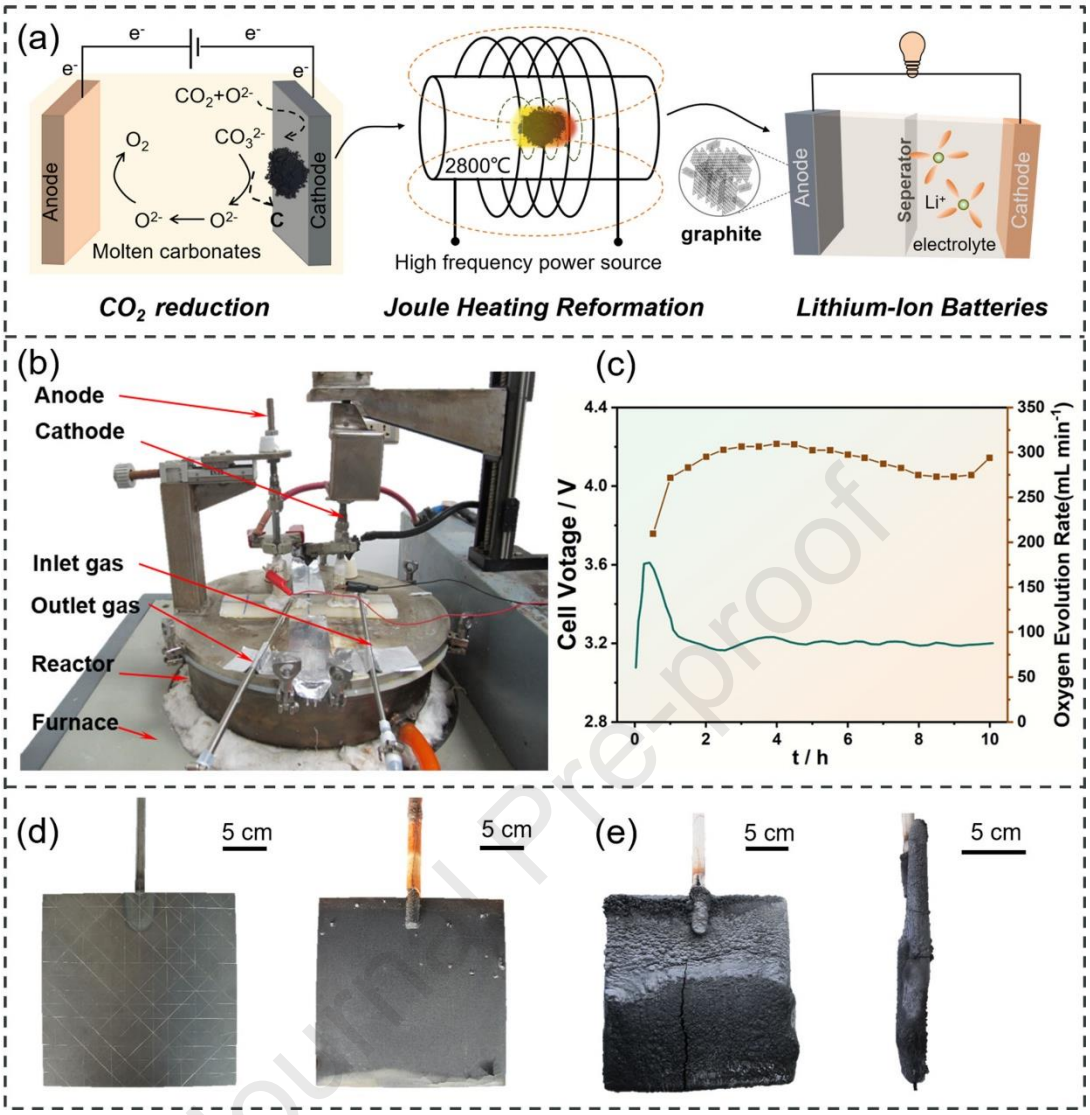

178

179 **Fig. 1.** 100-ampere-scale molten carbonates electrolysis cell for CO_2 electrochemical
180 reduction. (a) Schematic of CO_2 to high-quality graphite via molten salt electrolysis and
181 Joule heating reformation (b) Optical image of the 100-ampere-scale electrolysis cell;
182 (c) Variation in cell voltage and oxygen evolution rate during constant-current
183 electrolysis; (d) Optical images of the anode before (left) and after (right) electrolysis;
184 (e) Optical images of the cathode after electrolysis.

185 Fig. 1a clearly shows the schematic of CO_2 to high-quality graphite via high-
186 temperature molten salt electrolysis and Joule heating reformation. In the beginning, a
187 100-ampere-scale CO_2 electrolysis cell(Fig. 1b) was constructed, capable of capturing
188 and electrochemically converting 1 kilogram of CO_2 per day, using a eutectic salt
189 mixture of Li_2CO_3-Na_2CO_3-K_2CO_3 as the electrolyte, an iron electrode with a lithium

ferrite oxide film for high corrosion resistance as the oxygen evolution anode, and a nickel metal plate as the cathode. Electrolysis was performed at a constant current of 100 A for 10 h, with the cell voltage maintained at approximately 3.2 V as shown in Fig. 1c. CO_2 was introduced through a porous titanium sparger at the bottom of the molten salt electrolyte, forming bubbles around 100 μm in diameter, which were captured and absorbed by the molten salt, converting to CO_3^{2-}. The CO_3^{2-} ions were reduced to carbon material and O^{2-} at the cathode. After electrolysis, as presented in Fig. 1e, a dense black carbon layer, approximately 1 cm thick, formed on both sides of the cathode plate. After washing and drying, 93.49 g of CO_2-derived carbon was obtained, with a Coulombic efficiency of 83.5%. After electrolysis, the size of the anode(Fig. 1d) remained almost unchanged, and its surface was covered with a dense oxide film, indicating that this anode exhibits excellent corrosion resistance in the high-temperature molten salt system and can serve as an inert oxygen evolution anode for this system.

The structure and composition of the CO_2-derived carbon (EC) was further characterized. Fig. 2a shows the XRD patterns of CO_2-derived carbon. The broad peak at 26° and the weaker diffraction peak at 43° correspond to the (002) and (100) planes of aromatic layers[37], respectively, indicating that the CO_2-derived carbon is an amorphous carbon material. The Raman spectrum of CO_2-derived carbon (Fig. 2b) displays peaks at 1350 cm^{-1} (D band) and 1580 cm^{-1} (G band), associated with vibrations from disordered carbon atoms and ordered carbon atom plane layers, respectively. The I_D/I_G ratio of 0.96 indicates a high degree of disorder and defects, suggesting a low degree of graphitization. SEM images (Fig. 2d-e) reveal that the EC consists of agglomerated carbon particles ranging from 50 nm to 100 nm, forming a chaotic clustered structure and rough flake structure. This morphology relates to the formation mechanism of CO_2-derived carbon in carbonate molten salt electrolysis, where CO_3^{2-} ions are reduced at the cathode to form carbon atoms, which aggregate into carbon nanoparticles, further forming clustered and flake structures due to the molten salt template and metal cathode catalysis.

To improve the graphitization degree of the CO_2-derived carbon, high-frequency induction heating furnace was employed to generate Joule heating within the sample, heating it to 2800°C for thermal reformation. As shown in Fig. 2a, the XRD pattern of the CO_2-derived carbon after Joule heating reformed CO_2-derived carbon (EC-2800) exhibits a sharp diffraction peak near 26°, indicating that the carbon has been transformed into highly crystalline graphite. The Raman spectrum of the reformed carbon (Fig. 2b) shows a decreased I_D/I_G ratio of 0.04, lower than the reported 0.06 for artificial graphite prepared from petroleum coke through Joule heating reformation[24], indicating a highly ordered graphite crystal structure. SEM images (Fig. 2f) show that the reformed carbon mainly consists of smooth flake structures. TEM analysis (Fig. 2g) further confirms the presence of distinct graphite lattice fringes, with an interlayer spacing (d_{002}) estimated at about 0.35 nm, slightly larger than the 0.34 nm spacing of flake graphite. This larger interlayer spacing facilitates the rapid intercalation and deintercalation of Li^+ in EC-2800[38]. Additionally, the reformed carbon retains some disordered structures within the graphite lattice, which can enhance Li^+ diffusion through pseudocapacitive adsorption or intercalation, promoting effective lithium ion transport in the electrode microstructure[39].

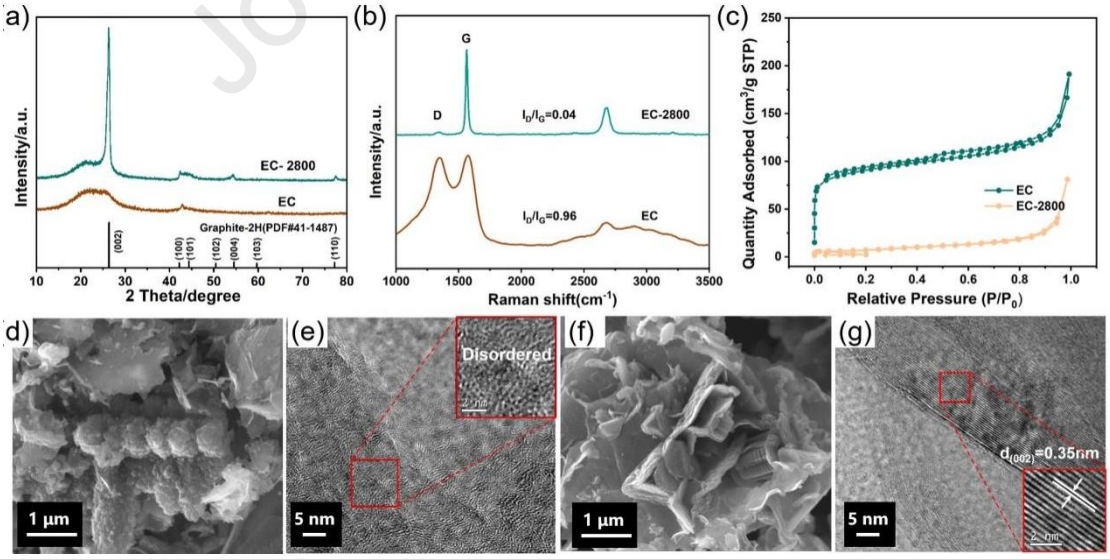

Fig. 2. Characterization of CO_2-derived carbon pre and post-Joule heating reformation. (a) XRD spectra; (b) Raman spectra; (c) Nitrogen isotherm adsorption-desorption curves; (d) SEM before reforming; (e) TEM before reforming; (f) SEM after reforming;

(g) TEM after reforming.

Furthermore, nitrogen adsorption-desorption tests were conducted on EC and EC-2800. The isotherm curves and pore size distributions are shown in Fig. 2c and Fig. S1. EC exhibits a typical type I curve, with a rapid increase in gas adsorption at low pressure, indicating abundant microporous structures. EC-2800 shows slight adsorption at relatively low pressure and a slower increase at medium to high pressure with minor hysteresis, indicating the presence of mesopores. The specific surface areas of EC and EC-2800, calculated by the BET method, are 334.85 and 28.9441 $m^2 g^{-1}$, respectively. The specific surface area of EC-2800 significantly decreases after Joule heating reformation. Detailed pore size parameter data are presented in Table 1.

Table 1 Specific surface area and pore size parameters of various samples

Samples	S_{BET} ($m^2 g^{-1}$)	Pore volume ($cm^3 g^{-1}$)	Average pore size (nm)
EC	334.8458	0.2957	3.4997
EC-2800	28.9441	0.1251	17.2951

In summary, we constructed a 100-ampere-scale molten salt CO_2 electrolysis cell, efficiently converting CO_2 into amorphous CO_2-derived carbon. The CO_2-derived carbon was thermally reformed into graphite material with excellent graphitization(EC-2800), using high-frequency inductive Joule heating.

3.2 Optimization of CO_2-derived graphite with asphalt and petroleum coke

To further enhance the particle size of Joule heating reformed CO_2-derived carbon and reduce the specific surface area, we conducted experiments by composite mixing of CO_2-derived carbon with asphalt and petroleum coke, followed by Joule heating reformed. Three sets of experiments were conducted with different ratios of asphalt, petroleum coke, and CO_2-derived carbon: 2:2:6, 2:4:4, and 2:6:2.

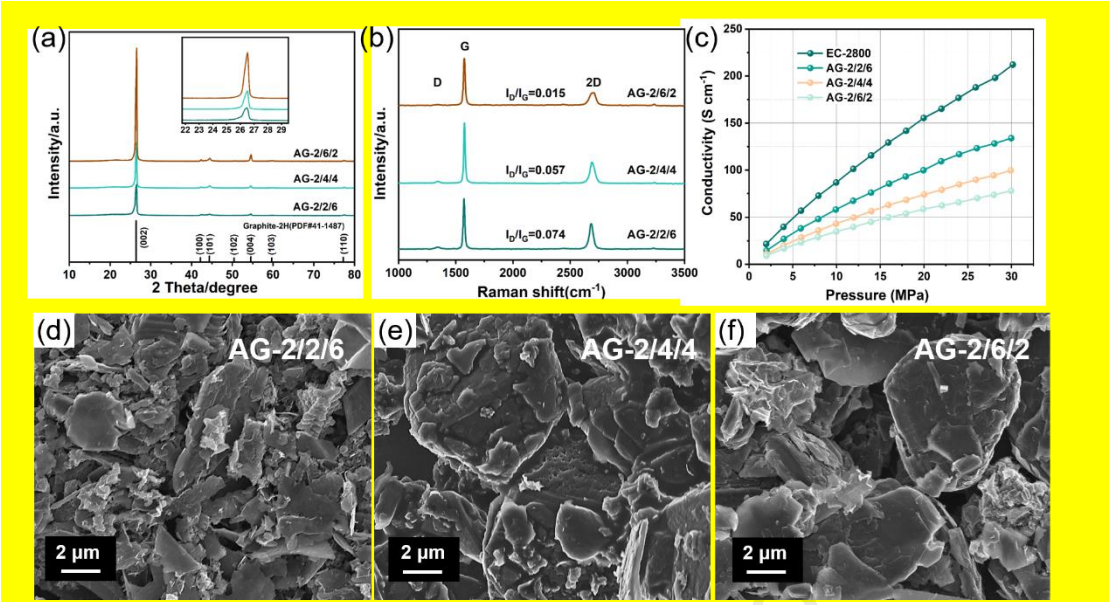

Fig. 3. Preparation of artificial graphite anodes with varying proportions of added CO_2-derived carbon. (a) XRD; (b) Raman spectroscopy; (c) Results of the conductivity; (d) SEM images of AG-2/2/6; (e) SEM images of AG-2/4/4; (f) SEM images of AG-2/6/2.

Fig. 3a shows the XRD patterns of CO_2-derived graphite. It is clear that CO_2-derived graphite synthesized with 20%, 40%, and 60% CO_2-derived carbon exhibits sharp diffraction peaks at 26°, resembling the peak characteristic of 2H graphite configuration, indicating a high degree of graphitization. Moreover, as the proportion of added petroleum coke increases, the intensity of the 26° diffraction peak of synthesized CO_2-derived graphite becomes stronger. Additionally, the graphitization degrees of AG-2/2/6, AG-2/4/4, and AG-2/6/2 were calculated using Bragg's equation, resulting in values of 88.89%, 91.78%, and 91.93%, respectively. Fig. 3b presents the Raman spectra of artificial graphite prepared with different amounts of added CO_2-derived carbon. The I_D/I_G values for AG-2/2/6, AG-2/4/4, and AG-2/6/2 are 0.074, 0.057, and 0.015, respectively, all indicating low values, demonstrating a highly perfect graphite microcrystalline structure and high degree of graphitization. Consistently, as the proportion of added petroleum coke increases, the I_D/I_G values decrease, which aligns well with the findings from XRD. The conductivity of all powders is shown in Figure 3(c). Under the same pressure conditions, EC-2800 exhibits the best conductivity, followed by AG-2/2/6, AG-2/4/4, and AG-2/6/2 in descending order. The

higher the proportion of CO_2-derived carbon added, the better the conductivity of the synthesized artificial graphite. Nitrogen adsorption-desorption isotherms (Fig. S2(a)) and pore size distributions (Fig. S2(b)) were obtained for artificial graphite with different proportions of added CO_2-derived carbon. According to the BET method, the specific surface areas of AG-2/2/6, AG-2/4/4, and AG-2/6/2 are 14.13, 10.97, and 7.96 $m^2 g^{-1}$, respectively. The higher the proportion of petroleum coke added, the smaller the specific surface area of the synthesized artificial graphite. The pore size distribution shows abundant micropores and mesopores with diameters less than 50 nm in all synthesized artificial graphites. Detailed pore size parameter data is presented in Table 2.

Table 2 Specific surface area and pore size parameters of various samples

Samples	S_{BET} ($m^2 g^{-1}$)	Pore volume ($cm^3 g^{-1}$)	Average pore size (nm)
AG-2/2/6	14.1306	0.0530	15.0144
AG-2/4/4	10.9683	0.0408	14.8748
AG-2/6/2	7.9574	0.0294	14.9479

SEM results (Fig. 3d-f) reveal that after the addition of asphalt and petroleum coke, Joule heating reformed CO_2-derived carbon transforms from a chaotic thin layer structure to smooth particle structures ranging from 2 to 10 μm. With increasing petroleum coke content, the scattered sheet structure of Joule heating reformed CO_2-derived carbon gradually decreases, and the completeness of particles increases, accompanied by a continuous decrease in specific surface area, consistent with the results of nitrogen adsorption-desorption tests. The addition of asphalt and petroleum coke bonds scattered CO_2-derived carbon into regular particles, enhancing the graphitization degree of the CO_2-derived graphite and significantly reducing its specific surface area.

3.3 Electrochemical performance of CO_2-derived graphite

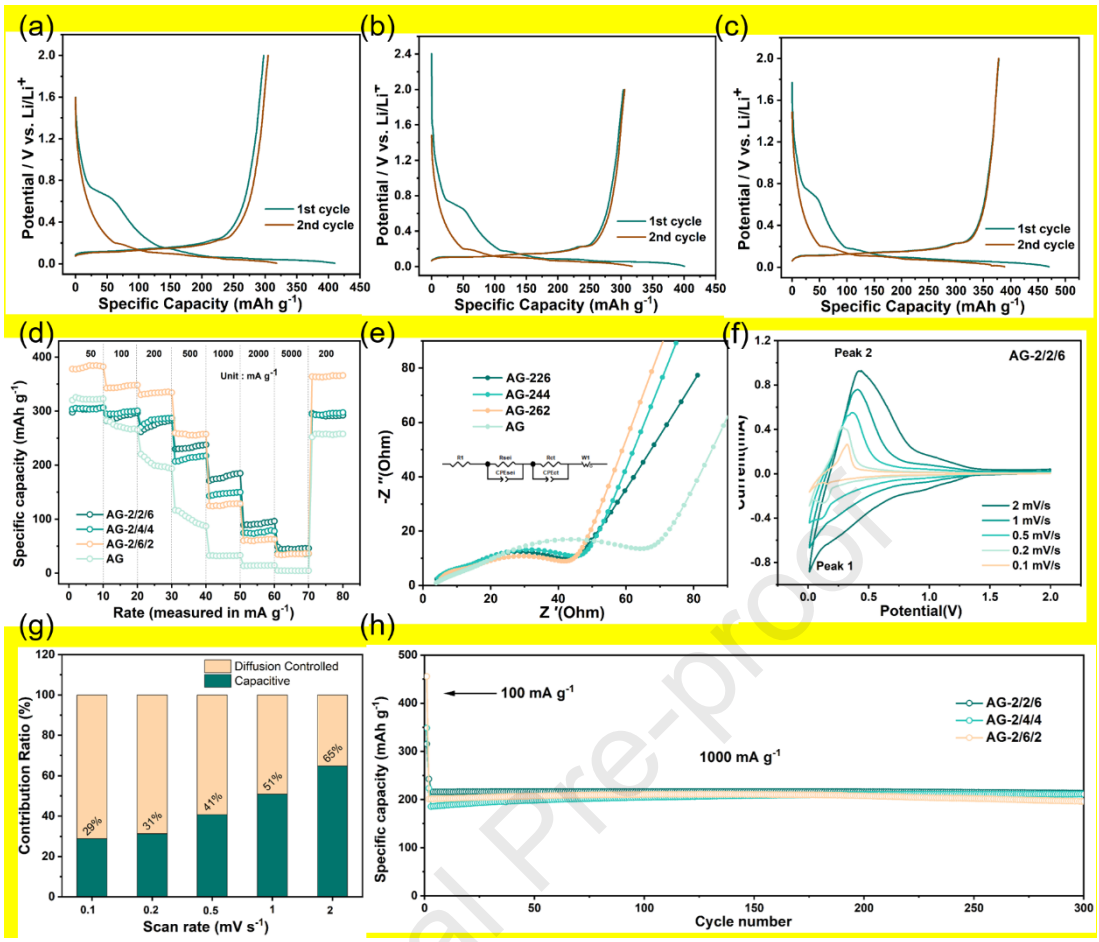

Fig. 4. Electrochemical performance of CO_2-derived graphite. (a) The charge-discharge curve of AG-2/2/6; (b) The charge-discharge curve of AG-2/4/4; (c) The charge-discharge curve of AG-2/6/2; (d) Rate capability; and (e) Nyquist plots for CO_2-derived graphite with different ratios of CO_2-derived carbon addition; (f) Cyclic voltammetry curves of AG-2/2/6 at various scan rates; (g) The capacitance and diffusion contribution ratios for AG-2/2/6 at different scan rates; and (h) Cycle performance chart of CO_2-derived graphite.

Fig. 4a-c shows the charge-discharge curves for AG-2/2/6, AG-2/4/4, and AG-2/6/2 as anode materials for lithium-ion batteries, with specific capacities of 297.7, 303.6, and 378.1 mAh g^{-1} at a current density of 50 mA g^{-1}, and initial Coulombic efficiencies of 72.6%, 75.8%, and 80.5%, respectively. The rate performance graph in Fig. 4d indicates that all three ratios of Joule heating reformed CO_2-derived carbon maintain excellent rate capability, achieving capacities of 184.4 mAh g^{-1}, 164.4 mAh

g^{-1}, and 148.6 mAh g^{-1} at a current density of 1A g^{-1}, which are significantly higher than the 32 mAh g^{-1} of commercial artificial graphite anodes (AG). This demonstrates that the Joule heating reformed CO_2-derived carbon anodes achieve high lithium storage capacity and excellent rate capability. This improvement is primarily attributed to the disordered structures retained within the reformed CO_2-derived carbon anodes, which form pore structures that enhance current uniformity and reduce polarization[40].

To further investigate the lithium intercalation kinetics of the Joule heating reformed CO_2-derived carbon with different proportions of CO_2-derived carbon, electrochemical impedance spectroscopy (EIS) was conducted on the de-intercalated graphite. The equivalent circuit fitting (Fig. 4e) shows that the SEI film resistances for AG-2/2/6, AG-2/4/4, AG-2/6/2 and the AG control group are 9.36 Ω, 9.96 Ω, 5.94 Ω and 16.09 Ω, respectively, and the charge transfer resistances are 29.87 Ω, 33.48 Ω, 35.23 Ω and 51.77 Ω, respectively. All three ratios exhibit low charge transfer resistance. Subsequent cyclic voltammetry tests at different scan rates for the AG-2/2/6 ratio (Fig, 4f-g) and the calculated pseudo-capacitance contributions during the lithium storage process indicate that AG-2/2/6 primarily exhibits diffusion-controlled behavior with minor capacitive contributions. At a scan rate of 1 mV s^{-1}, the pseudo-capacitance contribution ratio is 50.9%, suggesting a high reversible capacity from capacitive adsorption. Cyclic voltammetry results (Fig. S3a-c) further reveal that the peak shape of Peak 4 for the AG-2/2/6 graphite anode is more gradual compared to other ratios, indicating a more pronounced pseudo-capacitive effect and higher discharge capacity in the "sloping region"[39], consistent with the EIS results.

The cycling performance of Joule heating reformed CO_2-derived carbon with different compositions was tested (Figure 4(h)), showing that AG-2/2/6, AG-2/4/4, and AG-2/6/2 materials maintained their capacities without degradation after 300 cycles at a current density of 1 A g^{-1}, highlighting their excellent cycling stability. Besides, it appears that a higher proportion of CO_2-derived carbon carbon leads to better cycling performance for the artificial graphite, although the differences are not very pronounced.

This can be primarily attributed to the high degree of graphitization and fewer defects in AG-2/2/6, AG-2/4/4, and AG-2/6/2. This is attributed to the addition of CO_2-derived carbon, which facilitates Li^+ diffusion between graphite particles and reduces the pulverization and detachment of graphite particles during long-term cycling[41,42]. Additionally, the high conductivity of electrolyte carbon and its disordered structure reduce polarization and improve current uniformity, resulting in no significant degradation during cycling.

Finally, Figure S4(a) shows the charge-discharge curves at current densities of 0.1 C, 0.2 C, 0.5 C, and 1 C. Figure S4 (b) presents the rate performance of the full cell (AG-2/2/6 || LFP) , with a specific capacity of 151.6 mAh g^{-1} at 0.1 C and 136.5 mAh g^{-1} at 0.2 C. Figure S4 (c) illustrates the cycling performance at a current density of 0.5 C, with a capacity retention rate exceeding 88.7% after 120 cycles. This indicates that AG-2/2/6 still demonstrates considerable potential for applications in full cells.

In summary, the graphite anodes prepared by Joule heating reforming of CO_2-derived carbon combined with asphalt and petroleum coke exhibit high specific capacity, initial Coulombic efficiency, and excellent rate and cycling performance.

3.4 Mechanism of Joule heating reformation for CO_2-derived carbon

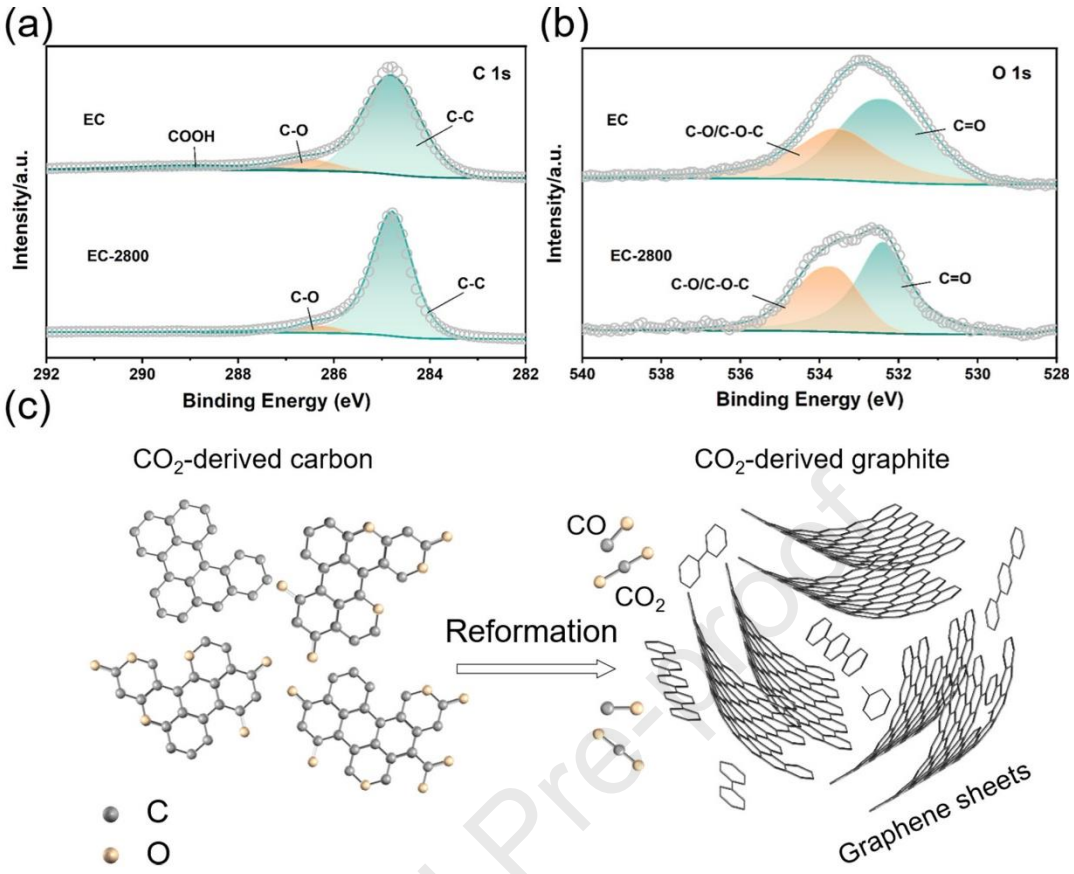

Fig. 5. XPS spectra of CO_2-derived carbon pre- and post-Joule heating reformation (a) C 1s (b) O 1s (c) Schematic of Joule heating reformation of CO_2-derived carbon

The primary mechanism of graphitization for soft carbon materials such as petroleum coke and asphalt during high-temperature thermal reformation involves the escape of hydrogen atoms at elevated temperatures. Hydrocarbons and aromatic compounds undergo dehydrogenation and subsequently reorganize into ordered graphite structures[43]. However, CO_2-derived carbon lacks hydrogen elements, and its Joule heating reformation mechanism remains unclear.

To investigate the mechanism of Joule heating reformation for CO_2-derived carbon, X-ray Photoelectron Spectroscopy (XPS) analysis was conducted on the carbon before and after Joule heating reformation (Fig. 5a-b, Fig. S5 and Table 3).The results indicate that the CO_2-derived carbon consists of 91.90 at.% carbon (C) and 8.10 at.% oxygen (O), with O 1s spectra showing 3.53 at.% C-O bonds and 4.57 at.% C=O bonds, and C 1s spectra revealing 74.36 at.% C-C bonds, 8.95 at.% C-O bonds, and 8.59 at.%

COOH groups, indicating a significant presence of oxygen within the carbon structure. This is likely due to the retention of oxygen elements as C-O-C bonds or other oxygen-containing functional groups during the reduction of CO_3^{2-} to carbon at the cathode in the preparation process[44].

Post Joule heating reformation, the CO_2-derived carbon shows an increased carbon content of 96.58 at.% and a reduced oxygen content of 3.42 at.%. The O 1s spectra now include 1.45 at.% C-O bonds and 1.97 at.% C=O bonds, while the C 1s spectra show 91.95 at.% C-C bonds and 4.63 at.% C-O bonds. The substantial reduction in oxygen content after reformation suggests that C-O-C bonds and surface oxygen-containing functional groups are disrupted, with oxygen being released as CO and CO_2. The deoxygenated carbon atoms and graphite microcrystals then rearrange into a graphite structure, driven by the principle of minimal energy under Joule heating[45,46].

AG-2/2/6 exhibits better rate performance, which is primarily due to its highest proportion of electrolyte carbon, retaining more disordered structures in the artificial graphite post-Joule heating reformation. From a conductivity perspective, the disordered structure provides more irregular connections on a microscopic level, facilitating faster electron conduction and thus improving rate performance[47]. Furthermore, from the viewpoint of ion diffusion, more disordered structures typically imply more complex porosity and defects, which create shorter diffusion paths for lithium ions during intercalation and deintercalation[48], enabling faster intercalation and deintercalation in AG-2/2/6 during high-rate charge-discharge processes.

Table 3 XPS analysis results for CO_2-derived carbon before and after Joule heating reformation

Sample	O (at%)	C (at%)	O 1s		C 1s		
			C-O/ C-O-C (at %)	C=O (at %)	C-C (at %)	C-O (at %)	COOH (at %)
EC	8.10	91.90	3.53	4.57	74.36	8.95	8.59
EC-2800	3.42	96.58	1.45	1.97	91.95	4.63	/

4. Conclusions.

In conclusion, this study successfully demonstrated the transformative potential of molten salt electrolysis for synthesizing high-quality CO_2-derived carbon materials, particularly in the form of graphitized graphite anodes for lithium-ion batteries. By establishing a 100-ampere-scale electrolysis cell, we efficiently produced significant quantities of amorphous CO_2-derived carbon, which were subsequently transformed into highly graphitized graphite through Joule heating at 2800 ^{o}C. The composite modification with asphalt and petroleum further optimized the material, reducing surface area and enhancing electrochemical performance. The CO_2-derived graphite anodes exhibited impressive specific capacities ranging from 297.7 to 378.1 mAh g^{-1}, coupled with initial Coulombic efficiencies between 72.6% and 80.5%. Notably, these anodes demonstrated excellent rate capability and stability over 300 charge-discharge cycles at a current density of 1 A g^{-1}. Finally, we assembled a coin full-cell using AG-2/2/6 anode and LFP cathode, which demonstrated good cycling performance. Mechanistic insights from XPS analysis revealed a significant reduction in oxygen content post-reformation, crucial for promoting the formation of highly graphitized structures. This research advances the fundamental understanding of CO_2-derived carbon synthesis and highlights its promising applications in sustainable energy technologies, particularly in lithium-ion battery technology. The developed approach not only addresses the environmental challenges associated with CO_2 emissions but also contributes to the development of high-performance energy storage solutions essential for future energy systems.

CRediT authorship contribution statement

Minghao Liu: Writing – original draft, Investigation, Formal analysis, Data curation, Software, Writing – review & editing, Conceptualization. **Hao shi**: Writing – review & editing, Visualization. **Lei guo**: Formal analysis, Data curation. **Zhouyu Fang**: Investigation. **Di Chen**: Resources. **Wenmiao Li**: Formal analysis, Methodology.

Bowen Deng: Writing – review & editing, Funding acquisition. **Wei Li**: Writing – review & editing, Funding acquisition. **Kaifa Du**: Conceptualization, Project administration, Funding acquisition, Writing – review & editing. **Huayi Yin**: Writing – review & editing, Funding acquisition. **Dihua Wang**: Conceptualization, Project administration, Funding acquisition.

Declaration of Competing Interest

The authors declare that they have no known competing financial interests or personal relationships that could have appeared to influence the work reported in this paper.

Funding sources

This work was supported by National Natural Science Foundation of China (Nos. 52031008, 51874211, 21673162, 51325102, U22B2071, 21703073, 22005225), International Science and Technology Cooperation Program of China (2015DFA90750), China Postdoctoral Science Foundation(2020M682468), and Young Elite Scientists Sponsorship Program by CAST(YESS20230100).

Data Availability

Data will be made available on request.

References:

[1] R. Yu, B. Deng, K. Zheng, X. Wang, K. Du, and D. Wang, A facile strategy to synthesize graphitic carbon-encapsulated core-shell nanocomposites derived from CO_2 as functional materials. Compos. Commun. 22 (2020) 100464. http://doi.org/10.1016/j.coco.2020.100464

[2] Z. Chen, Y. Gu, K. Du, X. Wang, W. Xiao, X. Mao, et al, Enhanced electrocatalysis performance of amorphous electrolytic carbon from CO_2 for oxygen reduction by surface modification in molten salt. Electrochim. Acta 253 (2017) 248-256.

http://doi.org/10.1016/j.electacta.2017.09.053

[3] D. Jiang, J. Yang, and D. Wang, Green carbon material for organic contaminants adsorption. Langmuir 36 (2020) 3141-3148. http://doi.org/10.1021/acs.langmuir.9b03811

[4] H.V. Ijije, R.C. Lawrence, and G.Z. Chen, Carbon electrodeposition in molten salts: electrode reactions and applications. RSC Adv. 4 (2014) 35808-35817. http://doi.org/10.1039/C4RA04629C

[5] M.A. Hughes, J.A. Allen, and S.W. Donne, Carbonate reduction and the properties and applications of carbon formed through electrochemical deposition in molten carbonates: A review. Electrochim. Acta 176 (2015) 1511-1521. http://doi.org/10.1016/j.electacta.2015.07.134

[6] B. Deng, H. Yin, K. Du, and D. Wang, Efficient molten salt CO_2 capture and selective electrochemical transformation processes toward carbon neutrality: advances, challenges, and prospects. Sci China Chem 66 (2023) 3116-3135. http://doi.org/10.1007/s11426-023-1826-3

[7] H. Yin, B. Deng, K. Du, W. Li, S. Gao, H. Shi, et al, High-temperature molten-salt electrochemical technologies for carbon neutralization, Chin. Sci. Bull. 68 (2023) 3998-4014, https://doi.org/10.1360/TB-2023-0190

[8] B. Deng, Z. Chen, M. Gao, Y. Song, K. Zheng, J. Tang, et al, Molten salt CO_2 capture and electro-transformation (MSCC-ET) into capacitive carbon at medium temperature: effect of the electrolyte composition. Faraday Discuss. 190 (2016) 241-258. http://doi.org/10.1039/c5fd00234f

[9] Y. Jia, Z. Zhou, D. Chen, E. Li, Z. Jiang, L. Zhao, et al, Recent advances in molten salt CO_2 capture and electrochemical conversion to functional carbon materials. J. Ind. Eng. Chem. 134 (2024) 17-27. http://doi.org/10.1016/j.jiec.2023.12.054

[10] S. Licht, A. Douglas, J. Ren, R. Carter, M. Lefler, and C.L. Pint, Carbon nanotubes produced from ambient carbon dioxide for environmentally sustainable lithium-ion and sodium-ion battery anodes. ACS Cent. Sci. 2 (2016) 162-168.

http://doi.org/10.1021/acscentsci.5b00400

[11] H. Wu, Z. Li, D. Ji, Y. Liu, L. Li, D. Yuan, et al, One-pot synthesis of nanostructured carbon materials from carbon dioxide via electrolysis in molten carbonate salts. Carbon 106 (2016) 208-217. http://doi.org/10.1016/j.carbon.2016.05.031

[12] H.V. Ijije, C. Sun, and G.Z. Chen, Indirect electrochemical reduction of carbon dioxide to carbon nanopowders in molten alkali carbonates: Process variables and product properties. Carbon 73 (2014) 163-174. http://doi.org/10.1016/j.carbon.2014.02.052

[13] A. Yu, G. Ma, J. Jiang, Y. Hu, M. Su, W. Long, et al, Bio-inspired and eco-friendly synthesis of 3D spongy meso-microporous carbons from CO_2 for supercapacitors. Chem. Eur. J. 27 (2021) 10405-10412. http://doi.org/10.1002/chem.202100998

[14] R. Yu, B. Deng, K. Du, D. Chen, M. Gao, and D. Wang, Modulating carbon growth kinetics enables electrosynthesis of graphite derived from CO_2 via a liquid–solid–solid process. Carbon 184 (2021) 426-436. http://doi.org /10.1016/j.carbon.2021.08.033

[15] L. Hu, Y. Song, S. Jiao, Y. Liu, J. Ge, H. Jiao, et al, Direct conversion of greenhouse gas CO_2 into graphene via molten salts Electrolysis. ChemSusChem 9 (2016) 588-594. http://doi.org/10.1002/cssc.201501591

[16] D. Tang, H. Yin, X. Mao, W. Xiao, and D.H. Wang, Effects of applied voltage and temperature on the electrochemical production of carbon powders from CO_2 in molten salt with an inert anode. Electrochim. Acta (2013) 567-573. https://doi.org/10.1016/j.electacta.2013.10.109

[17] B.P. Thapaliya, A.S. Ivanov, H. Chao, M. Lamm, M. Chi, H.M. Meyer, et al, Molten salt electrochemical upcycling of CO_2 to graphite for high performance battery anodes. Carbon 212 (2023) 118151. http://doi.org/10.1016/j.carbon.2023.118151

[18] W. Ding, H. Ren, Z. Li, M. Shang, Y. Song, W. Zhao, et al., Tuning Surface

Rock‐Salt Layer as Effective O Capture for Enhanced Structure Durability of LiCoO2at 4.65 V, Adv Energy Mater. 13 (2024) http://doi.org/10.1002/aenm.202303926

[19] W. Zheng, G. Liang, H. Guo, J. Li, J. Zou, J. A. Yuwono, et al., Enhancing the reaction kinetics and structural stability of high-voltage LiCoO2 via polyanionic species anchoring, Energ Environ Sci. 12 (2024) 4147-56. http://doi.org/10.1039/D4EE00726C

[20] M. Li, J. Lu, Z. Chen, and K. Amine, 30 Years of lithium-ion batteries. Adv. Mater. 30 (2018). http://doi.org/10.1002/adma.201800561

[21] J. Xu, X. Cai, S. Cai, Y. Shao, C. Hu, S. Lu, et al, High-energy lithium-ion batteries: recent progress and a promising future in applications. Energy Environ. Mater. 6 (2023). http://doi.org/10.1002/eem2.12450

[22] L. Li, D. Zhang, J. Deng, Y. Gou, J. Fang, H. Cui, et al, Carbon-based materials for fast charging lithium-ion batteries. Carbon 183 (2021) 721-734. http://doi.org/10.1016/j.carbon.2021.07.053

[23] C. Fan, H. He, K. Zhang, and S. Han, Structural developments of artificial graphite scraps in further graphitization and its relationships with discharge capacity. Electrochim. Acta 75 (2012) 311-315. http://doi.org/10.1016/j.electacta.2012.05.010

[24] Z. Liu, Y. Shi, Q. Yang, H. Shen, Q. Fan, and H. Nie, Effects of crystal structure and electronic properties on lithium storage performance of artificial graphite. RSC Adv. 13 (2023) 29923-29930. http://doi.org/10.1039/d3ra05785b

[25] J. Wang, J. Liu, Y. Wang, C. Wang, and Y. Xia, Pitch modified hard carbons as negative materials for lithium-ion batteries. Electrochim. Acta 74 (2012) 1-7. http://doi.org/10.1016/j.electacta.2012.03.099

[26] H. Qin, Z. Mo, J. Lu, X. Sui, Z. Song, B. Chen, et al, Ultrafast transformation of natural graphite into self-supporting graphene as superior anode materials for lithium-ion batteries. Carbon 216 (2024) 118559.

http://doi.org/10.1016/j.carbon.2023.118559

[27] Y. Zhao, Y. Fu, Y. Meng, Z. Wang, J. Liu, and X. Gong, Challenges and strategies of lithium-ion mass transfer in natural graphite anode. Chem. Eng. J 480 (2024) 148047. http://doi.org/10.1016/j.cej.2023.148047

[28] H. Groult, B. Kaplan, F. Lantelme, S. Komaba, N. Kumagai, H. Yashiro, et al, Preparation of carbon nanoparticles from electrolysis of molten carbonates and use as anode materials in lithium-ion batteries. Solid State Ionics 177 (2006) 869-875. http://doi.org/10.1016/j.ssi.2006.01.051

[29] J. Ge, L. Hu, W. Wang, H. Jiao, and S. Jiao, Electrochemical conversion of CO_2 into negative electrode materials for Li-ion batteries. ChemElectroChem 2 (2014) 224-230. http://doi.org/10.1002/celc.201402297

[30] J. Tang, B. Deng, F. Xu, W. Xiao, and D. Wang, The lithium storage performance of electrolytic-carbon from CO_2. J. Power Sources 341 (2017) 419-426. http://doi.org/10.1016/j.jpowsour.2016.12.037

[31] L. Xie, C. Tang, Z. Bi, M. Song, Y. Fan, C. Yan, et al, Hard carbon anodes for next-generation Li-ion batteries: review and perspective. Adv. Energy Mater. 11 (2021). http://doi.org/10.1002/aenm.202101650

[32] Z. Tang, S. Zhou, Y. Huang, H. Wang, R. Zhang, Q. Wang, et al, Improving the initial Coulombic efficiency of carbonaceous materials for Li/Na-ion batteries: origins, solutions, and perspectives. Electrochem. Energy Rev 6 (2023). http://doi.org/10.1007/s41918-022-00178-y

[33] X. Ding, Z. He, J. Li, X. Xu, Z. Li, Carbon carrier-based rapid Joule heating technology: a review on the preparation and applications of functional nanomaterials, Nanoscale. 26 (2024) 1239-12328. http://doi.org/10.1039/d4nr01510j

[34] J. Yuan, Y. Zhang, F. Chen, Z. Gu, An overview of Joule heating in energy storage materials and applications, J MATER CHEM C. (2024) http://doi.org/10.1039/D4TC01736F

[35] D. An, K. H. Kim, C. Lim, Y. Lee, Effect of kneading and carbonization temperature on the structure of the carbon block for thermally conductive bulk graphites, Carbon Lett. 6 (2021) 1357-64. http://doi.org/10.1007/s42823-021-00288-5

[36] G. Centi, G. Iaquaniello, and S. Perathoner, Can we afford to waste carbon dioxide? carbon dioxide as a valuable source of carbon for the production of light olefins. ChemSusChem 4 (2011) 1265-1273. http://doi.org/10.1002/cssc.201100313

[37] B. Xing, C. Zhang, Y. Cao, G. Huang, Q. Liu, C. Zhang, et al, Preparation of synthetic graphite from bituminous coal as anode materials for high performance lithium-ion batteries. Fuel Process. Technol. 172 (2018) 162-171. http://doi.org/10.1016/j.fuproc.2017.12.018

[38] C. Zhong, S. Weng, Z. Wang, C. Zhan, and X. Wang, Kinetic limits and enhancement of graphite anode for fast-charging lithium-ion batteries. Nano Energy. 117 (2023) 108894. http://doi.org/10.1016/j.nanoen.2023.108894

[39] W. Bergh, and M. Stefik, Understanding rapid intercalation materials one parameter at a Time. Adv. Funct. Mater. 32 (2022). http://doi.org/10.1002/adfm.202204126

[40] H. Groult, B. Kaplan, S. Komaba, N. Kumagai, V. Gupta, T. Nakajima, et al, Lithium insertion into carbonaceous anode materials prepared by electrolysis of molten Li-K-Na carbonates. J. Electrochem. Soc. 150 (2003) G67-G75. http://doi.org/10.1149/1.1531490

[41] J. Wang, J. Liu, Y. Wang, C. Wang, and Y. Xia, Pitch modified hard carbons as negative materials for lithium-ion batteries. Electrochim. Acta 74 (2012) 1-7. http://doi.org/10.1016/j.electacta.2012.03.099

[42] C. Ge, Z. Fan, J. Zhang, Y. Qiao, J. Wang, and L. Ling, Novel hard carbon/graphite composites synthesized by a facile *in situ* anchoring method as high-performance anodes for lithium-ion batteries. RSC Adv. 8 (2018) 34682-34689. http://doi.org/10.1039/C8RA07170E

[43] H. Zeng, B. Xing, Y. Cao, B. Xu, L. Hou, H. Guo, et al, Insight into the microstructural evolution of anthracite during carbonization-graphitization process from the perspective of materialization. Int. J. Min. Sci. Technol 32 (2022) 1397-1406. http://doi.org/10.1016/j.ijmst.2022.06.009

[44] X. Mao, Z. Yan, T. Sheng, M. Gao, H. Zhu, W. Xiao, et al, Characterization and adsorption properties of the electrolytic carbon derived from CO_2 conversion in molten salts. Carbon 111 (2017) 162-172. http://doi.org/10.1016/j.carbon.2016.09.035

[45] X. Tang, F. Xie, Y. Lu, Z. Chen, X. Li, H. Li, et al, Intrinsic effects of precursor functional groups on the Na storage performance in carbon anodes. Nano Res. 16 (2023) 12579-12586. http://doi.org/10.1007/s12274-023-5643-9

[46] M. Song, Z. Yi, R. Xu, J. Chen, J. Cheng, Z. Wang, et al, Towards enhanced sodium storage of hard carbon anodes: Regulating the oxygen content in precursor by low-temperature hydrogen reduction. Energy Storage Mater. 51 (2022) 620-629. http://doi.org/10.1016/j.ensm.2022.07.005

[47] H. Zhang, Y. Yang, D. Ren, L. Wang, X. He, Graphite as anode materials: Fundamental mechanism, recent progress and advances, Energy Stor. (2021) 147-70. http://doi.org/10.1016/j.ensm.2020.12.027

[48] M. Weiss, R. Ruess, J. Kasnatscheew, Y. Levartovsky, N. R. Levy, P. Minnmann, et al., Fast Charging of Lithium‐Ion Batteries: A Review of Materials Aspects, Adv Energy Mater. 33 (2021) 2101126. http://doi.org/10.1002/aenm.202101126

Declaration of interests

☒ The authors declare that they have no known competing financial interests or personal relationships that could have appeared to influence the work reported in this paper.

☐ The authors declare the following financial interests/personal relationships which may be considered as potential competing interests: